Controllable Assembly of WO_3 Nanorods/Nanowires into Hierarchical Nanostructures

Zhanjun Gu,[†,‡] Tianyou Zhai,[†] Bifen Gao,[†] Xiaohai Sheng,[†] Yaobing Wang,[†] Hongbing Fu,[†] Ying Ma,*[,†] and Jiannian Yao*[,†]

Beijing National Laboratory for Molecular Sciences, Key Laboratory of Photochemistry, Institute of Chemistry, Chinese Academy of Sciences, Beijing (100080), Peoples Republic of China, and Graduate School of the Chinese Academy of Science, Beijing (100080), Peoples Republic of China

Received: August 10, 2006; In Final Form: September 19, 2006

The controlled synthesis of two novel h-WO_3 hierarchical structures made of nanorods/nanowires has been successfully realized in a large scale via a simple hydrothermal method. It is demonstrated that the morphology of the final products is significantly influenced by adding different sulfates. The urchinlike and ribbonlike structures of WO_3 can be selectively prepared by adding Rb_2SO_4 and K_2SO_4, respectively. The morphology evolvement and the growth mechanism were studied carefully. The sulfate-induced oriented attachment growth mechanism has been proposed for the possible formation mechanism of the ribbonlike sample. For urchinlike products, two growing stages are believed to be involved in the growth process. The current understanding of the growth mechanism of these nanostructures may be potentially applied for designing other oriented or hierarchical nanostructures based on 1D nanoscale building blocks through the direct solution-growth.

1. Introduction

Assembly of functional nanoscale building blocks into an appropriate superstructure is an important prerequisite for electronic and optoelectronic applications of nanocrystals.[1,2] Nanotubes, nanowires, nanorods, and nanobelts represent a very unique class of one-dimensional (1D) nanoscale building blocks. Once such one-dimensional nanoscale building blocks can be ordered and rationally assembled into appropriate two- or three-dimensional architectures, they will offer fundamental scientific opportunities for investigating the influence of size and dimensionality with respect to their collective optical, magnetic, and electronic properties and would provide possibilities to probe brand-new properties and applications resulting from the spatial orientation and arrangement of the nanocrystals.[3−6] Many efforts have been focused on the integration of nanorods/ nanowires as building blocks into 2D or 3D complex superstructures,[7−12] and several hierarchical structures, such as ZnS nanowire bundles,[13,14] penniform $BaWO_4$ nanostructures,[15] and dandelion-like CuO architectures[16] have been successfully obtained in the past few years. However, it remains a significant challenge to develop facile, solution-based, and shape-controlled self-assembly routes for the formation of hierarchical architectures from 1D nanocrystals.

As an important fundamental material, WO_3 has attracted great interest due to its interesting physical properties and potential wide-ranging applications. Recently, a number of methods have been developed for the preparation of one-dimensional tungsten oxides, such as electrochemical techniques,[17] template directed synthesis,[18,19] solution-based colloidal approach,[20,21] and chemical vapor deposition[22−24] and hydrothermal reactions.[25,26] Very recently, Niederberger reported a growth and assembly of crystalline tungsten oxide nanostructures assisted by bioligation.[27] However, the synthesis of WO_3 nanorod/nanowires and simultaneous organization them into well-defined 2D and 3D nanostructures is still a challenge. In our previous work, highly oriented nanowire bundles of WO_3 have been prepared by hydrothermal treatment of the WO_3 (sol) in the presence of Li_2SO_4.[28] Thus, it is anticipated that other ordered superstructures or hierarchical architectures based on 1D WO_3 nanocrystals could be obtained by varying the experimental conditions.

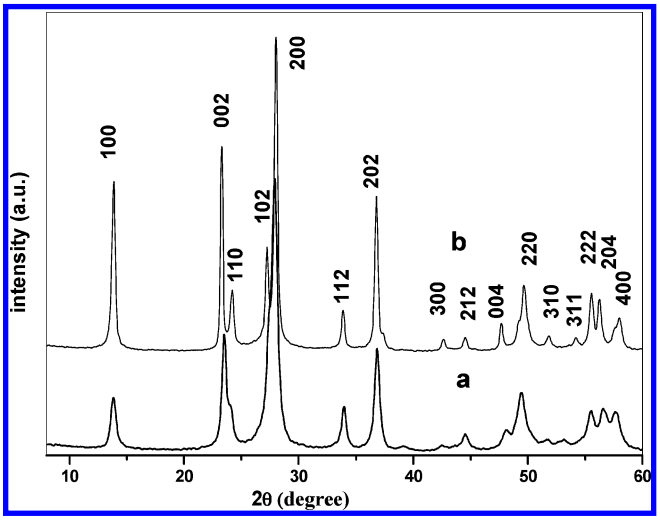

Figure 1. XRD patterns of the as-prepared WO_3 products. (a) Urchinlike sample. (b) Ribbonlike sample.

Herein, we report a simple approach to actualize the shape- and assembly-controlled synthesis of WO_3 nanocrystals. The urchinlike and ribbonlike superstructures based on 1D nanoscale building blocks have been selectively prepared by adding different sulfates under hydrothermal conditions. The morphology evolvement and the growth mechanism were studied carefully. To the best of our knowledge, this is the first report on a controllable hydrothermal synthetic method for the selective growth and assembly of tungsten oxide nanorods/nanowires into well-defined two- and three-dimensional nanostructures.

* Corresponding author. Fax (+86)10-82616517. Tel: (+86)10-82616517. E-mail: jnyao@iccas.ac.cn (J. N. Yao).
† Beijing National Laboratory for Molecular Sciences.
‡ Graduate School of the Chinese Academy of Science.

10.1021/jp065170y CCC: $33.50
Published on Web 10/28/2006

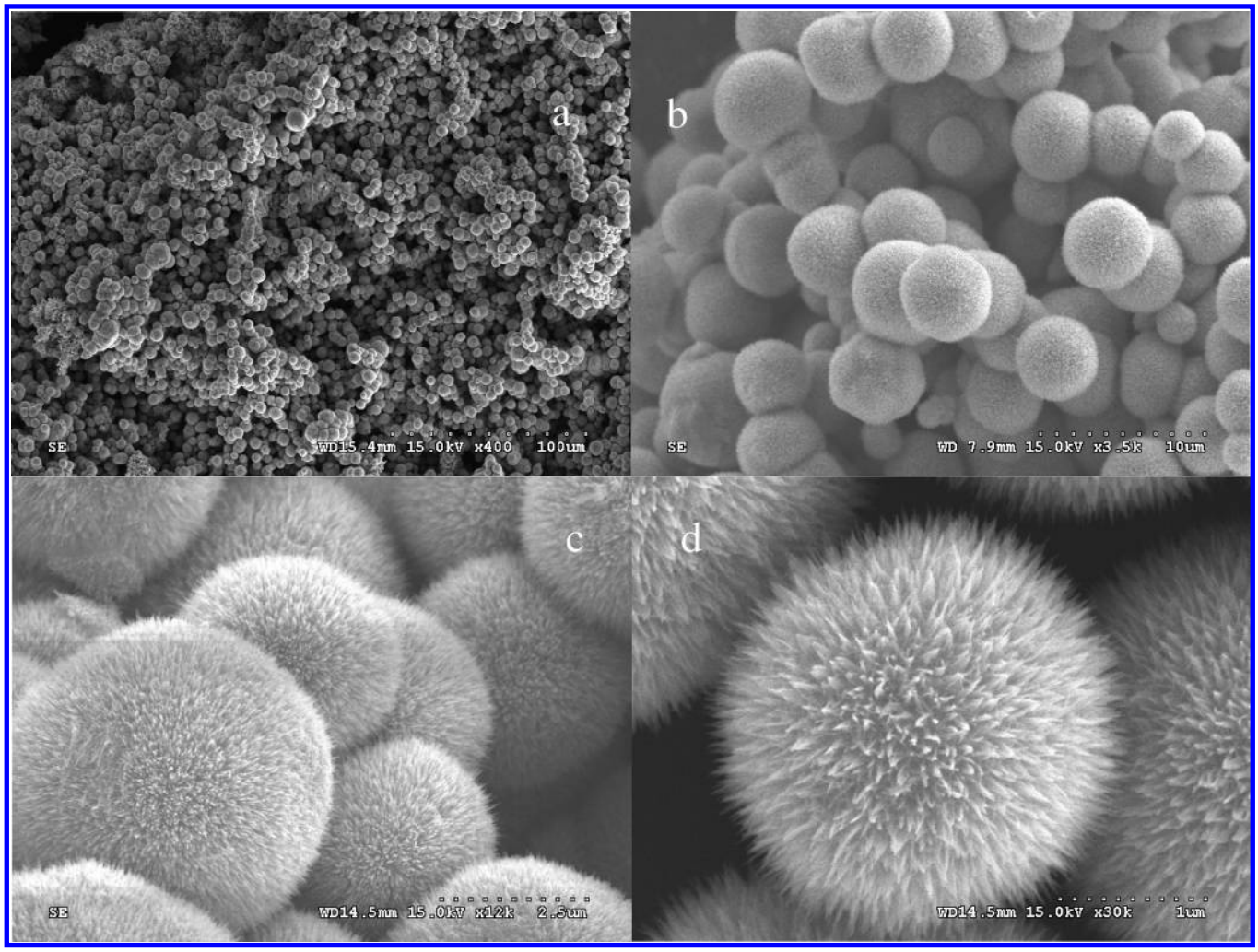

Figure 2. (a−d) The SEM images of the urchinlike structures with different magnification. The products were prepared in the presence of 0.3 g of Rb_2SO_4.

2. Experimental Section

Materials. All the chemicals were of analytical grade and used without further purification. Potassium sulfate (K_2SO_4), rubidium sulfate (Rb_2SO_4), oxalic acid ($H_2C_2O_4$), and sodium tungstate (Na_2WO_4) were purchased from Beijing Chemical Reagent Company.

Synthesis. In a typical experiment, WO_3 sol was prepared in advance as follows: sodium tungstate powder (8.15 g, 0.025 mol) was dissolved in distilled water (100 mL). Then Na_2WO_4 solution was acidified to a pH range of 1−1.2 using HCl (3 mol L^{-1}) solution. A white precipitate was generated. $H_2C_2O_4$ (6.3 g) was added to the mixture and diluted to 250 mL. After that, a translucent, homogeneous, and stable WO_3 sol was formed. A 20 mL volume of WO_3 sol was transferred to a 25-mL autoclave, and then Rb_2SO_4 (0.3 g) was added to the solution, sealed, and maintained at 180 °C for 2−72 h. Then the precipitates were filtered, washed sequentially with water and ethanol to remove ions possibly remnant in the final products, and dried at 60 °C. Following the above procedures, high purity of urchinlike WO_3 nanostructures were obtained on a large scale. The whole process can be easily adjusted to prepare h-WO_3 with ribbonlike structures by simply adding K_2SO_4 (1 g) instead of Rb_2SO_4 while keeping other conditions unchanged. To study the formation process of the nanostructures, the experimental parameters have been varied during the synthesis.

Characterization. XRD analysis was performed using a Japan Riyaku D/max-2500 diffractometer with Cu Kα radiation ($\lambda = 1.5418$ Å). The sizes and shapes of the nanostructures were observed on a field emission scanning electron microscope (SEM, Hitachi, S-4300) and high-resolution transmission electron microscope (HRTEM, JEOL JEM-2010 operated at 200 kV).

3. Results and Discussion

The h-WO_3 nanorod-based microspherical assemblies can be selectively prepared in the presence of Rb_2SO_4. X-ray diffraction (XRD) pattern of the as-obtained products is shown in Figure 1a. All the diffraction peaks can be indexed to the pure hexagonal phase of WO_3 with lattice constants of $a = 7.340$ Å and $c = 7.668$ Å, which agrees well with the reported values ($a = 7.324$ Å, $c = 7.662$ Å) from the JCPDS card (85-2460). No peaks of impurities were detected from this pattern. The peaks are strong and narrow, indicating good crystallinity of the as-prepared samples. The morphology and microstructures of the sample analyzed in Figures 2 and 3 were investigated using SEM and TEM. Figure 2a is a low-magnification scanning electron microcopy (SEM) image, which clearly shows that there exists a great deal of h-WO_3 microspheres with diameters ranging from several to tens of microns. The magnified SEM images (Figure 2b and 2c) show that the surfaces of these spherical structures are covered by many nanorods and take on an urchinlike appearance. More careful observation of a typical

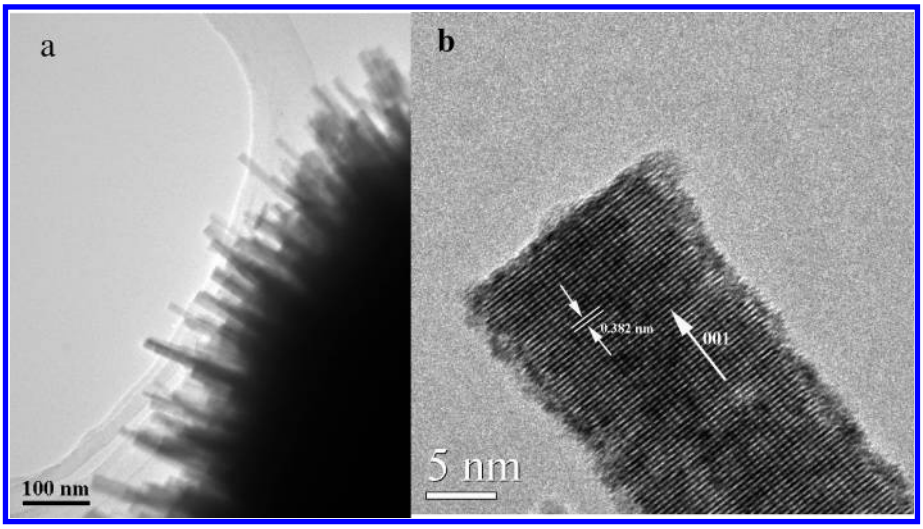

Figure 3. (a) TEM image of the product. (b) HRTEM image of the tip of an individual nanorod from a microsphere.

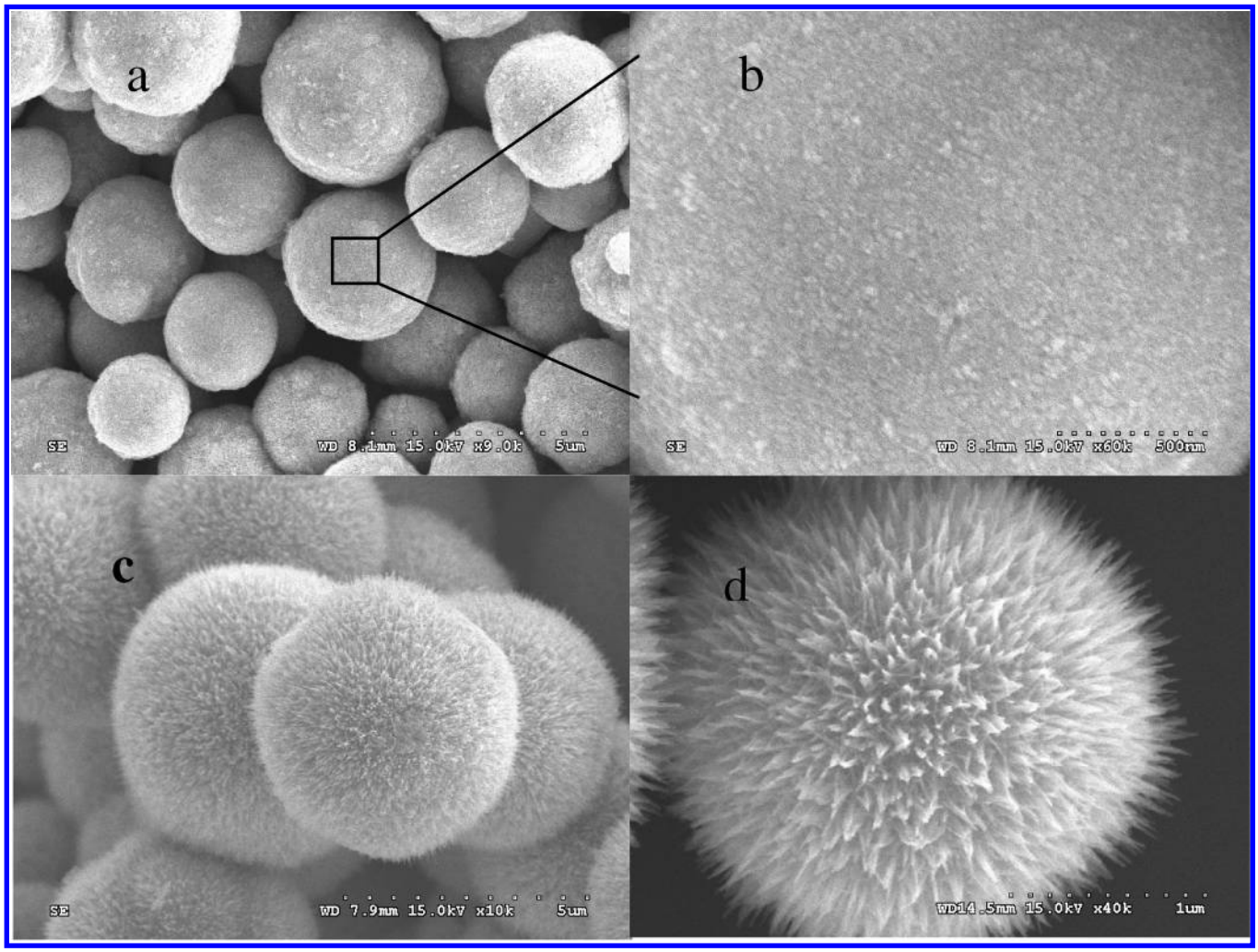

Figure 4. SEM images of the intermediates of the h-WO_3 urchinlike structures collected at different times. (a) 1 h. (b) A detailed view of the surface of the sphere in part a. (c) 2 h. (d) 4 h.

urchinlike structure, shown in Figure 2d, indicates that numerous nanorods with very high density grow pointing toward the center of the sphere. More detail of morphological and structural features was studied using TEM. These nanorods have uniform diameters of 5−25 nm, illustrated in Figure 3a. The spacing of the lattice fringes are found to be about 0.382 Å, as shown in Figure 3b. This plane can be well indexed as (002) plane of the h-WO_3 crystal, confirming that the nanowires are single crystals grown along the *c*-axis.

To investigate the growth process of the WO_3 hierarchical structures, we conducted experiments for different reaction times. Two obvious evolution stages could be clearly observed, as shown in the Figure 4. At the early stages, an examination of the intermediate products collected after 1 h showed that there

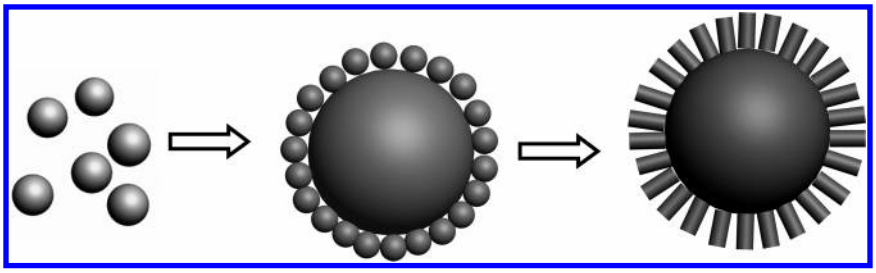

Figure 5. Schematic illustration detailing all major steps and changes involved in the formation of WO_3 urchinlike structures.

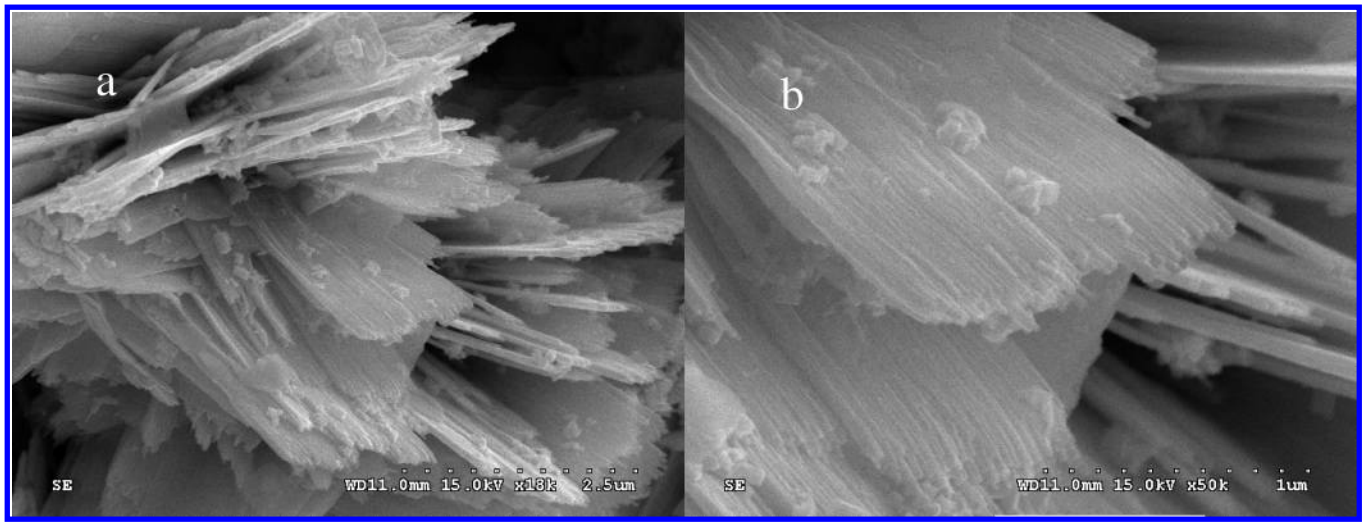

Figure 6. SEM images of h-WO_3 nanoplates prepared by adding 1 g of Rb_2SO_4. (a) Overall product morphology. (b) A detailed view on an individual nanoplate.

existed a great deal of spherical particles, and their surfaces were covered by small nanoparticles, as shown in Figure 4a and 4b. While the intermediates collected after 2 h were spherical particles, their surfaces were wholly covered by small nanorods (Figure 4c). It was clear that the nanorods on the surface of the big sphere were grown from the surface nanoparticles of the big spheres. After reaction for 4 h, uniform nanorods with typical lengths of 200−500 nm were grown from the surface of the spheres and finally formed the urchinlike structures, shown in Figure 4d. Two kinds of intermediates revealed that there were two growth stages during the formation of the urchinlike structures. One facilitated the growth of aggregate particles, and the latter facilitated the growth of 1D nanorods. Based on the above experimental results, the formation process of the hierarchical structures can be illustrated as follows: in the initial stages, the nanoparticles were quickly built and spontaneously aggregate to large spheres to minimize their surface area. As the reaction proceeds, the concentration of the nanoclusters decreases sharply due to the formation of large particles. As a result, the crystal growth stage transfers to a kinetically controlled process. Subsequent crystal growth is initiated preferentially from the active nanoparticles on the surfaces of the spheres, owing to the high concentration of SO_4^{2-} surrounding them. In other words, during the second stages, SO_4^{2-} may act as capping agent to preferentially adsorb on the faces parallel to the *c* axis of the WO_3 nanocrystal, leading to the formation of *c*-axis oriented nanorods. Figure 5 summarizes all major steps and changes involved in the formation of the WO_3 urchinlike structures. Similar cases have also been encountered in the synthesis of Pt and MnO_2 nanorod-based microspheres.[29,30]

The amount of Rb_2SO_4 also plays an important role in controlling the morphology of the final products. The urchinlike products could only be obtained in the presence of the low concentration of Rb_2SO_4. When the amount of Rb_2SO_4 was increased to 1 g, the nanoplates emerged (Figure 6a). Close observation shown in Figure 6b reveals that these nanoplates are composed of large numerous, highly aligned, and closely packed nanowires. The formation process of the nanoplate is obviously different from that of the urchinlike samples. This indicates that the high concentration of sulfate tends to induce the oriented aggregation of the nanorods.

The ribbonlike assemblies of h-WO_3 can be selectively prepared in the presence of K_2SO_4. In Figure 1b, powder XRD measurements show that the sample is phase-pure hexagonal structured WO_3 with lattice constants of $a = 7.334$ Å and $c = 7.658$ Å, which agrees well with the reported values from JCPDS card (85-2460). The morphologies of the as-synthesized products obtained by adding 1 g K_2SO_4 are shown in Figure 7, which reveal that the products exhibit exclusively 1D ribbonlike nanostructures with widths typically in the range of 100−1000 nm and lengths of up to tens of microns. The thickness of the ribbons ranges between 10 and 25 nm, as estimated from the Figure 7b and Figure 7c. These nanoribbons are all very thin and of high aspect ratio. The selected area electron diffraction (SAED) pattern shown in Figure 7d indicates that the nanoribbons are single crystal, whose long axis corresponds to the ⟨001⟩ direction.

To understand the formation mechanism of the ribbonlike products, we conducted the experiment in the presence of the different amount of K_2SO_4 while keeping other conditions unchanged. Comparative experiments have shown that without K_2SO_4, only irregular particles were obtained. When 0.3 g of K_2SO_4 was added to the solution, the h-WO_3 nanowires with diameters of 5−25 nm and lengths of 2 um were generated, as shown in Figure 8a. With an increase in the dosage of K_2SO_4 to 0.5 g, the ribbonlike nanostructures became predominant products (Figure 8b). Close observation shown in Figure 8c and

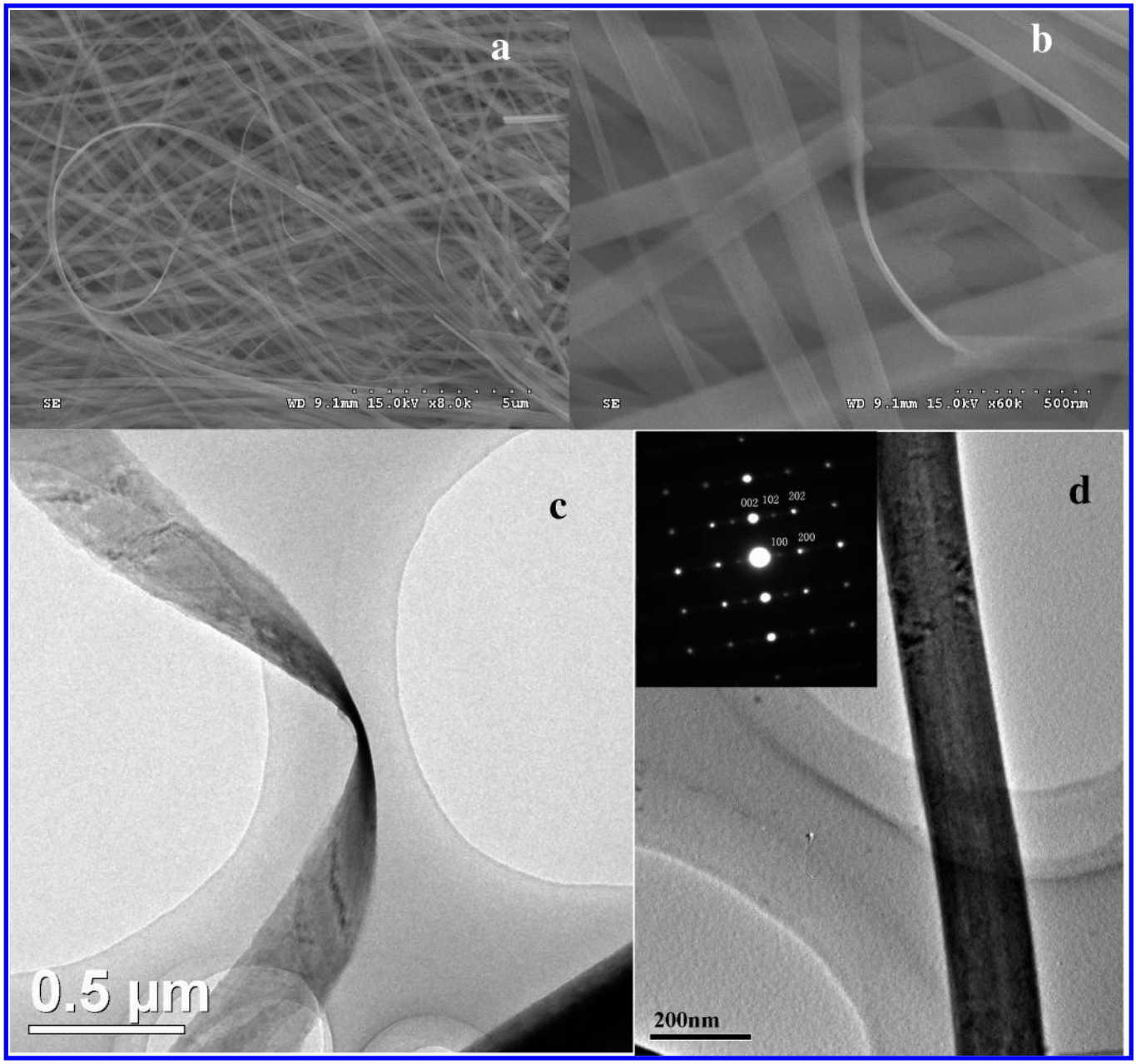

Figure 7. (a, b) SEM images of the ribbonlike products obtained by adding 1 g K_2SO_4. (c, d) TEM observation of the ribbonlike samples. Inset shows the diffraction of the nanoribbon. The clear lattice fringes indicate that the nanoribbon is single crystal and grows along [001] direction.

8d revealed that these ribbon-shape products are actually formed by the oriented attachment of large, numerous, highly aligned, and closely packed nanowires. From the diffraction pattern recorded from a ribbon, the single-crystal pattern clearly indicates the orientation alignment among all of the nanowires in the belt along [001], and they share the same side surface. (Figure 8e) These nanowires are aligned not only in length direction but also in crystallography orientation. This is a key characteristic of the sample. Also, edge defects at the interface between the two primary building block particles could be detected clearly, as indicated with an arrow in Figure 8g.The nanoribbons with regular shapes can be obtained by adding 1 g of K_2SO_4, as presented in Figure 8h. The HRTEM image of the sample is shown in Figure 8i. The parallelism of the lattice fringes demonstrates that these nanowires have fused into larger "ribbon" crystals and therefore provides direct evidence for the oriented-attachment growth mechanism. Also, many structural defects were observed in some regions of the nanoribbon. These microstructural features yield important clues to mechanisms by which primary building blocks assemble to produce larger nanoribbons. On the basis of these observations, it may be concluded that the ribbonlike nanostructures of h-WO_3 actually evolved from the oriented attachment of the primary h-WO_3 nanowires, and the presence of an appropriate amount of sulfate plays a key role in the formation of the h-WO_3 nanowires as well as the simultaneous assembly into ribbonlike superstructures. It is noted that the oriented-attachment mechanism originally put forward by Penn and Banfield has been applied to explain the growth of various oriented and hierarchical nanostructures via self-assembly of nanocrystals.[31−38] In this mechanism, primary particles may aggregate in an oriented fashion to produce a larger single crystal, or they may aggregate randomly and reorient, recrystallize, or undergo phase transformations to produce larger single crystals. In the so formed aggregates, the crystalline lattice planes may be almost perfectly aligned, or dislocations at the contact areas between the adjacent particles lead to defects in the final crystals. The current formation of ribbonlike structures of WO_3 via self-assembly of

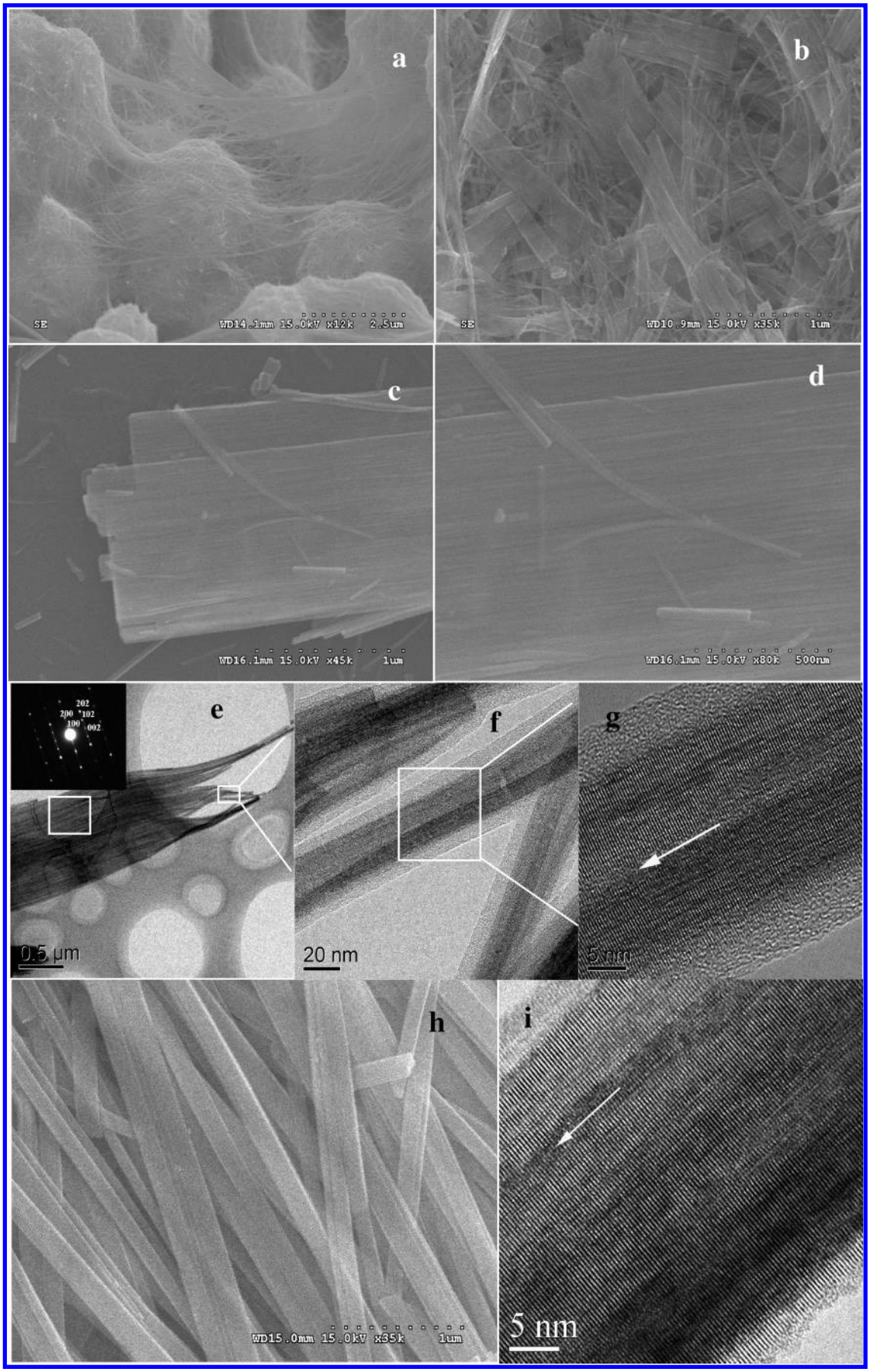

Figure 8. SEM images, TEM images, ED pattern, and HRTEM images of the sample obtained by adding different amount of K_2SO_4. (a) SEM image of the sample prepared in the presence of 0.3 g of K_2SO_4. (b−g) The SEM, TEM, and HRTEM images of as-synthesized WO_3 nanoribbons obtained by adding 0.5 g of K_2SO_4. Inset of part e shows the electron diffraction patterns of e. (h, i) SEM and HRTEM images of WO_3 nanoribbons obtained by adding 1 g of K_2SO_4. Many defects were observed in some region of the nanoribbon.

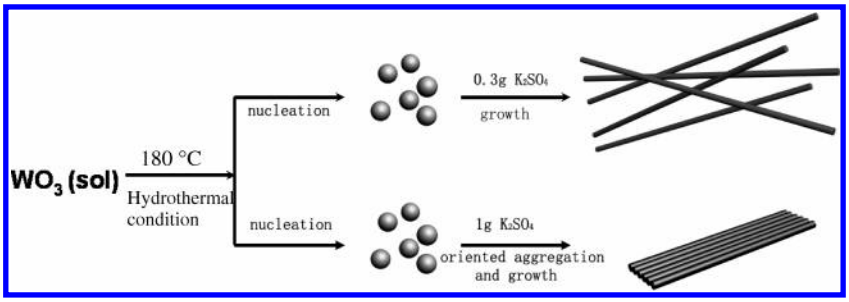

Figure 9. Schematic illustration of the formation process of WO_3 nanowires and ribbonlike nanostructures.

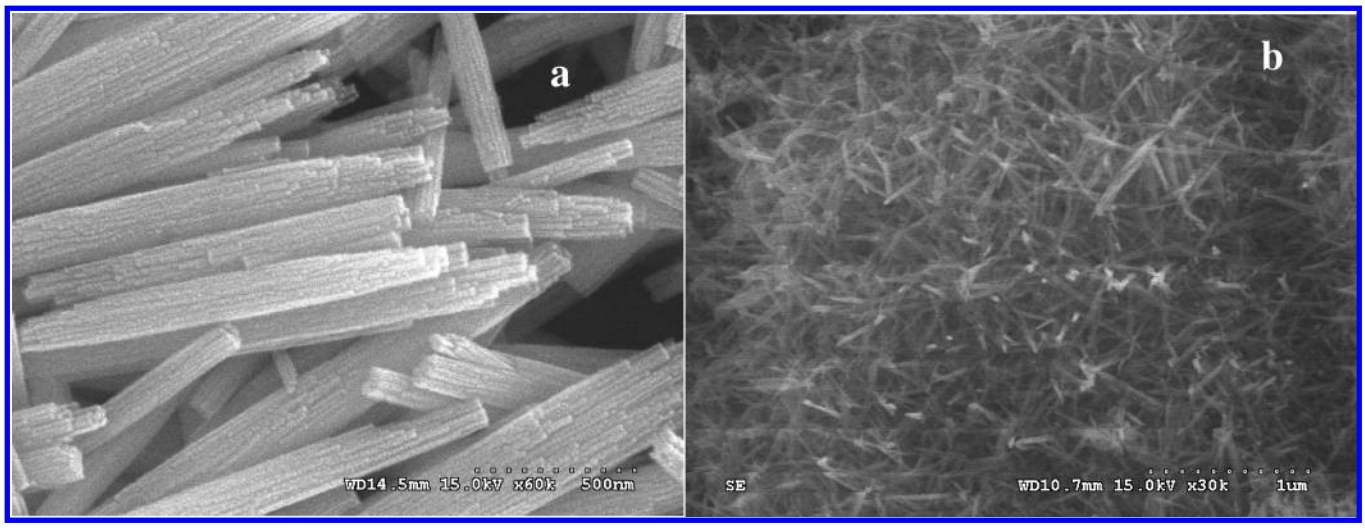

Figure 10. (a) Cylindrical nanowires bundles of WO_3 synthesized with 1 g of Na_2SO_4 at 180 °C for 8 h. (b) WO_3 nanorods prepared by adding 2 g of $(NH_4)_2SO_4$ at 180 °C for 8 h.

nanorods may represent another example of the oriented attachment. Figure 9 summarizes all major steps and changes involved in the formation of the WO_3 nanostructures.

On the basis of the above experiment, it is obvious that the sulfates play a key role in controlling the morphology of final products. Other alkali metal sulfates, such as Na_2SO_4, Li_2SO_4, and $(NH_4)_2SO_4$, were also tested in this work. Our results show that the addition of Na_2SO_4 or Li_2SO_4[28] leads to the formation of the cylindrical nanowires bundles, While only nanorods were generated by adding $(NH_4)_2SO_4$. (Figure 10) Currently, the shape-controlled assembly mechanism is still unclear. However, it is believed that the inherent growth habit of the crystals as well as the specific interaction between the sulfates and the crystal surfaces may have played an important role in control the morphology of the final crystals. Maybe, the different radius of Rb^+ and K^+ cations induce the different interactions between these cations and WO_3 nanocrystals, which leads to the different morphologies of the products. Other inorganic salts, including NaCl, KCl, LiBr, and KNO_3, have been tested in this work. Our results show that the addition of these inorganic salts only leads to the irregular WO_3 particles. We also found that the oxalic acid plays a crucial role in ensuring the formation of WO_3 nanorod-based superstructures. Without oxalic acid, only irregularly aggregated nanorods were obtained. This indicates that $H_2C_2O_4$ could induce and greatly enhance the directing role of sulfates in the preparation of tungsten oxide superstructures. More in-depth studies are necessary to further understand their growth process, which can provide important information for structure design and morphology-controlled synthesis of WO_3 and other oxides.

4. Conclusions

In summary, we have demonstrated a facile one-step, wet-chemical, self-assembly route for the selective creation of urchinlike and ribbonlike nanostructures based on 1D h-WO_3 nanocrystals. The formation mechanisms of ribbonlike and urchinlike structures have been investigated, and the sulfates have been found to clearly contribute to the creation of such structures. Other WO_3 nanostructures, such as cylindrical nanowires bundles and nanorods, could also be selectively prepared by adding Na_2SO_4 and $(NH_4)_2SO_4$, respectively. In addition, this synthetic method is very simple, mild, and controllable, and it provides a novel method for direct solution-growth of highly oriented and hierarchical nanostructures based on 1D nanoscale building blocks.

Acknowledgment. This work was supported by National Natural Science Foundation of China (No.50221201, 90301010, 50502033) and the Chinese Academy of Sciences.

References and Notes

(1) (a) Whitesides, G. M.; Grzybowski, B. *Science* **2002**, *295*, 2418. (b) Cölfen, H.; Antonietti, M. *Angew. Chem., Int. Ed.* **2005**, *44*, 5576. (c) Yu, S. H.; Cölfen, H. *J. Mater. Chem.* **2004**, *14*, 2124.

(2) Park, S.; Lim, J. H.; Chung, S. W.; Mirkin, C. A. *Science* **2004**, *303*, 348.

(3) Huang, Y.; Duan, X. F.; Wei, Q. Q.; Lieber, C. M. *Science* **2001**, *291*, 630.

(4) Wei, B. Q.; Vajtai, R.; Jung, Y.; Ward, J.; Zhang, R.; Ramanath, G.; Ajayan, P. M. *Chem. Mater.* **2003**, *15*, 1598.

(5) Patzke, G. R.; Krumeich, F.; Nesper, R. *Angew. Chem., Int. Ed.* **2002**, *41*, 2446.

(6) Li, M.; Schnablegger, H.; Mann, S. *Nature* **1999**, *402*, 393.

(7) Mo, M.; Yu, J. C.; Zhang, L. Z.; Li, S. K. A. *Adv. Mater.* **2005**, *17*, 756.

(8) Li, Z. Q.; Ding, Y.; Xiong, Y. J.; Xie, Y. *Cryst. Growth Des.* **2005**, *5*, 1953.
(9) Yuan, J. K.; Li, W. N.; Gomez, S.; Suib, S. L. *J. Am. Chem. Soc.* **2005**, *127*, 14184.
(10) Liu, B.; Yu, S. H.; Li, L. J.; Zhang, Q.; Zhang, F.; Jiang, K. *Angew. Chem., Int. Ed.* **2004**, *43*, 4745.
(11) Geng, J.; Zhu, J. J.; Chen, H. Y. *Cryst. Growth Des.* **2006**, *6*, 321.
(12) Shen, G. Z.; Bando, Y.; Lee, C. J. *J. Phys. Chem. B* **2005**, *109*, 10578.
(13) Moore, D. F.; Ding, Y.; Wang, Z. L. *J. Am. Chem. Soc.* **2004**, *126*, 14372.
(14) Zhu, Y. C.; Bando, Y.; Xue, D. F.; Golberg, D. *Adv. Mater.* **2004**, *16*, 831.
(15) Shi, H. T.; Ma, J. M.; Cheng, H. M. *J. Am. Chem. Soc.* **2003**, *125*, 3450.
(16) (a) Liu, B.; Zeng, H. C. *J. Am. Chem. Soc.* **2004**, *126*, 8124. (b) Lou, X. W.; Zeng, H. C. *J. Am. Chem. Soc.* **2003**, *125*, 2697.
(17) Gu, G.; Zheng, B.; Han, W. Q.; Roth, S.; Liu, J. *Nano Lett*. **2002**, *2*, 849.
(18) Lakshmi, B. B.; Dorhout, P. K.; Martin, C. R. *Chem. Mater.* **1997**, *9*, 857.
(19) Satishkumar, B. C.; Govindaraj, A.; Nath, M.; Rao, C. N. R. *J. Mater. Chem.* **2000**, *10*, 2115.
(20) Lee, K.; Seo, W. S.; Park, J. T. *J. Am. Chem. Soc.* **2003**, *125*, 3408.
(21) Hudson, M. J.; Peckett, J. W.; Harris, P. J. F. *J. Mater. Chem.* **2003**, *13*, 445.
(22) (a) Li, B.; Bando, Y.; Golberg, D. *Adv. Mater.* **2003**, *15*, 1294. (b) Liu, Z. W.; Bando, Y.; Tang, C. C. *Chemical Physics Lett.* **2003**, *372*, 179.
(23) Klinke, C.; Hannon, J. B.; Gignac, L.; Reuter, K.; Avouris, P. *J. Phys. Chem. B* **2005**, *109*, 17787.
(24) York, A. P. E.; Sloan, J.; Green, M. L. H. *Chem. Commun* **1999**, 269.
(25) Li, X. L.; Liu, J. F.; Li, Y. D. *Inorg. Chem.* **2003**, *42*, 921.
(26) Lou, X. W.; Zeng, H. C. *Inorg. Chem.* **2003**, *42*, 6169.
(27) (a) Polleux, J.; Gurlo, A.; Barsan, N.; Weimar, U.; Antonietti, M.; Niederberger, M. *Angew. Chem., Int. Ed.* **2005**, *45*, 261. (b) Polleux, J.; Pinna, N.; Antonietti, M.; Niederberger, M. *J. Am. Chem. Soc.* **2005**, *127*, 15595.
(28) Gu, Z. J.; Ma, Y.; Yang, W. S.; Zhang, G. J.; Yao, J. N. *Chem. Commun.* **2005**, 3597−3599.
(29) Chen, J. Y.; Herricks, T.; Geissler, M.; Xia, Y. N. *J. Am. Chem. Soc.* **2004**, *126*, 10854−10855.
(30) (a) Li, Z. Q.; Ding, Y.; Xiong, Y. J.; Xie, Y. *Cryst. Growth Des.* **2005**, *5*, 1953−1958. (b) Li, Z. Q.; Ding, Y.; Xiong, Y. J.; Yang, Q.; Xie, Y. *Chem. Commun.* **2005**, 918.
(31) (a) Penn, L. R.; Banfield, J. F. *Science* **1998**, *281*, 969. (b) Penn, R. L.; Oskam, G.; Strathmann, T. J.; Searson, P. C.; Stone, A. T.; David, R. V. *J. Phys. Chem. B* **2001**, *105*, 2177. (c) Banfield, J. F.; Welch, S. A.; Zhang, H. Z.; Ebert, T. T.; Penn, R. L. *Science* **1998**, *289*, 751.
(32) Peng, W. Q.; Qu, S. C.; Cong, G. W.; Wang, Z. G. *Cryst. Growth Des.* **2006**, *6*, 1518.
(33) Yang, H. G.; Zeng, H. C. *Angew. Chem., Int. Ed.* **2004**, *43*, 5930.
(34) Zhang, D. F.; Sun, L. D.; Yin, J. L.; Yan, C. H.; Wang, R. M. *J. Phys. Chem. B* **2005**, *109*, 8786.
(35) Shi, H. T.; Wang, X. H.; Zhao, N.; Qi, L. M.; Ma, J. M. *J. Phys. Chem. B*, **2006**, *110*, 748. (b) Shi, H. T.; Qi, L. M.; Ma, J. M.; Cheng, H. M.; Zhu, B. Y. *Adv. Mater.* **2003**, *15*, 1647.
(36) Chen, D.; Tang, K. B.; Li, F. Q.; Zheng, H. G. *Cryst. Growth Des.* **2006**, *6*, 247.
(37) Liu, B.; Zeng, H. C. *J. Am. Chem. Soc.* **2005**, *125*, 4430.
(38) (a) Cho, K. S.; Talapin, D. V.; Gaschler, W.; Murray, C. B. *J. Am. Chem. Soc.* **2005**, *127*, 7140.